Effects of kinetic resonances on the stability of resistive wall modes in reversed field pinch

D. Yadykin[1], Y.Q. Liu[2], R. Paccagnella[3]

[1] Euratom/VR Fusion Association, Chalmers University of Technology, Gothenburg, S-41296, Sweden

[2]Euratom/CCFE Fusion Association, Culham Science Centre, Abingdon, OX14 3DB, UK

[3] Consorzio RFX, Corso Stati Uniti 4, Padova, 35127, Italy

E-mail: dimitriy@chalmers.se

Abstract. The kinetic effects, due to the mode resonance with thermal particle drift motions in the reversed field pinch (RFP) plasmas, are numerically investigated for the stability of the resistive wall mode, using a non-perturbative MHD-kinetic hybrid formulation. The kinetic effects are generally found too weak to substantially change the mode growth rate, or the stability margin, re-enforcing the fact that the ideal MHD model is rather adequate for describing the RWM physics in RFP experiments.

PACS numbers: 52.35.Py, 28.52.Av, 52.55.Fa, 52.65.Kj

Submitted to: *Plasma Phys. Control. Fusion*

1. Introduction

Understanding physics and stabilization of the resistive wall mode (RWM) is of significant importance for the successful operation of the present day and the future fusion devices. Converted from the ideal MHD mode in the presence of the wall with finite electrical conductivity, and growing on the time scale of the magnetic field penetration time through the wall, the RWM sets pressure limit in the high beta, long pulse scenarios of the tokamak devices [1, 2, 3]. It also limits the discharge duration of the reversed field pinch (RFP) devices [4, 5, 6]. Control of the mode growth is necessary for the discharge time longer than the wall time.

Generally two methods are envisaged for the RWM stabilization: active control and stabilization via the mode resonance with continuum spectra or particle motions. For active control, the perturbed magnetic field, measured by a set of sensors, is used to generate the control signal for a set of active magnetic coils. This technique has been extensively studied theoretically [7, 8, 9, 10, 11, 12, 13, 14] and has been successfully applied in the present day fusion devices, allowing operations with the plasma pressure exceeding the no-wall limit for tokamaks, [15, 16, 17] and resulting in substantial increase of the plasma discharge duration in RFPs [18, 19] . These experiments also demonstrated the possibility of simultaneous suppression of multiple unstable modes, with different toroidal harmonic numbers.

The RWM suppression via the mode resonance with stable waves or particles is another possible control mechanism (also called passive stabilization). It has been experimentally observed in multiple tokamak configurations [20] that the mode is stabilized when the plasma rotation frequency is sufficiently high. Several physics mechanisms have been proposed, that can contribute to this stabilization. In the ideal MHD description, the free energy dissipation is caused by the mode resonance with the Alfvén [21, 22] or sound [23, 24] wave continuum spectra. The dissipation strength depends on the toroidal rotation frequency Ω of the plasma. In the absence of other damping, normally a rotation speed of the order of a few percent of the Alfvén speed is required for the full mode suppression. Another mechanism, that can contribute to the RWM stabilization, is associated with the ion Landau damping of the parallel sound wave. An accurate description of this mechanism requires kinetic treatment of the ion motion along magnetic field lines [25]. A fluid approximation can be made by adding a viscous force to the parallel momentum equation [26]. A large aspect ratio drift kinetic calculation was performed in Ref. [27], where the mode resonance with the transit motion of circulating and the bounce motion of trapped thermal ions were considered. The resulting kinetic terms were implemented as a semi-kinetic damping model [28] and subsequently improved [29]. In the regime of slow plasma rotation, where the rotation frequency is below the diamagnetic frequency of thermal particles, a damping model was proposed based on the mode resonance with the magnetic precession drift of trapped particles [30]. This model seems to predict well the observed RWM stabilization in DIII-D plasmas with balanced beam injection [31], as well as in recent NSTX experiments

[32]. The accurate prediction of the RWM stabilization for slowly rotating plasmas is an important issue for the future reactor experiment ITER.

Previous studies of the passive stabilization of the RWM were performed mainly for the tokamak configuration. In a RFP device, the poloidal and toroidal equilibrium magnetic fields are of the same order of magnitude. The toroidal field normally changes sign near the plasma edge. This normally results in a rich spectrum of the modes along the toroidal angle. Several non-resonant harmonics, with different toroidal mode numbers (positive or negative according to the sign of the safety factor q), can be simultaneously unstable and grow on the time scale comparable with the wall response time, and therefore are classified as the RWMs. Available theoretical results for the RFP configuration [33, 34] show that a plasma rotation frequency, in the range of the Alfvén frequency ($\Omega \sim \omega_a$), is needed for the mode suppression. Such a high plasma rotation is not observed in the present day RFP devices. Therefore, passive stabilization mechanism was not considered as realistic for RFPs. On the other hand, the mode resonance with particle drift motions also occurs in RFP plasmas in the slow rotation regime, and it is not clear to which degree the kinetic effects can contribute to the RWM stabilization in RFP configurations. In this work, numerical study of the effect of kinetic resonances on the RWM stability is performed for RFP plasmas. In particular, plasma parameters corresponding to the RFX device [35] are assumed.

2. Physics models and numerical schemes

In this section we briefly describe the physics models that are used in the present work. More complete description can be found in [36]. The stability of the RWM for these studies is determined by solving numerically the system of MHD equations with a drift kinetic closure, in the presence of the toroidal plasma flow

$$(-i\omega + in\Omega)\xi = \mathbf{v} + (\xi \cdot \nabla\Omega)R^2\nabla\phi \tag{1}$$

$$\rho(-i\omega + in\Omega)\mathbf{v} = -\nabla \cdot \mathbf{p} + \mathbf{j} \times \mathbf{B} + \mathbf{J} \times \mathbf{Q} - \rho[2\Omega\hat{\mathbf{Z}} \times \mathbf{v} + (\mathbf{v} \cdot \nabla\Omega)R^2\nabla\phi] - \nabla \cdot \mathbf{\Pi} \tag{2}$$

$$(-i\omega + in\Omega)\mathbf{Q} = \nabla \times (\mathbf{v} \times \mathbf{B}) + (\mathbf{Q} \cdot \nabla\Omega)R^2\nabla\phi \tag{3}$$

$$(-i\omega + in\Omega)p = -\mathbf{v} \cdot \nabla P \tag{4}$$

$$\mathbf{j} = \nabla \times \mathbf{Q} \tag{5}$$

where $\omega = i\gamma - \omega_r$ is the complex mode frequency, with γ being the mode growth or damping rate and ω_r being the real mode rotation frequency (in the laboratory frame), $\mathbf{B}$,$\mathbf{J}$,P- equilibrium magnetic field, current density and pressure respectively, $\hat{\mathbf{Z}}$ - unit vector in the vertical direction, ρ - plasma density, Ω - plasma rotation frequency in the toroidal direction ϕ, ξ,$\mathbf{v}$,$\mathbf{j}$,$\mathbf{Q}$ - plasma displacement, perturbed velocity, perturbed current, and perturbed magnetic field respectively, $\mathbf{p}$ - the perturbed pressure tensor.

The kinetic terms are coupled to the MHD equations via the pressure tensor terms,

defined as

$$\mathbf{p} = \mathbf{I}p + p_{\parallel}\hat{\mathbf{b}}\hat{\mathbf{b}} + p_{\perp}(\mathbf{I} - \hat{\mathbf{b}}\hat{\mathbf{b}}) \tag{6}$$

where p is the fluid pressure perturbation, associated with the "adiabatic" part of the drift kinetic solution, $p_{\parallel}, p_{\perp}$ are the parallel and perpendicular components of the kinetic pressure tensor, respectively, $\hat{\mathbf{b}} = \mathbf{B}/B$, $B =\mid \mathbf{B} \mid$, $\mathbf{I}$ is the unit tensor. For a perturbation with the given toroidal mode number n, the parallel and perpendicular components of the pressure tensor are calculated as:

$$p_{\parallel}e^{-i\omega t+in\phi} = \sum_{e,i}\int dv M v_{\parallel}^2 f_L^1 \tag{7}$$

$$p_{\perp}e^{-i\omega t+in\phi} = \sum_{e,i}\int dv \frac{1}{2} M v_{\perp}^2 f_L^1 \tag{8}$$

Here the summation is over the electron and ion species. The integration is carried out over the particle velocity space. M is the particle mass, $v_{\parallel}, v_{\perp}$ are the parallel and perpendicular velocity components, respectively, with respect to the equilibrium magnetic field. f_L^1 is the "non-adiabatic" part of the perturbed particle distribution function. It is derived as

$$f_L^1 = -f_{\epsilon}^0 \epsilon_k e^{-i\omega t+in\phi}\sum_{m,l} X_m H_{ml}\lambda_{ml} e^{-in\tilde{\phi}(t)+im<\dot{\chi}>+il\omega_b t} \tag{9}$$

where the subscripts n,m,l mark the Fourier components along the toroidal, poloidal angles and along the particle bounce orbit, f_{ϵ}^0 - derivative of the equilibrium distribution function (taken to be Maxwellian for thermal particles) with respect to the particle energy ϵ, ϵ_k - kinetic energy of the particles, H_{ml} - geometrical factor associated with the equilibrium quantities in the perturbed particle Lagrangian, λ_{ml} - the mode-particle resonance operator, $\tilde{\phi}(t) = \phi(t) - <\dot{\phi}> t$ - the periodic part (in bounce period) of the particle phase angle along the toroidal direction. $<\cdot>$ here denotes average over the particle bounce period. $\chi(t)$ is the particle poloidal phase angle. X_m denotes the poloidal Fourier harmonics of the perpendicular fluid displacement and the magnetic field perturbation. The mode-particle resonant operator is

$$\lambda_{ml} = \frac{n[\omega_{*N} + (\epsilon_k - 3/2)\omega_{*T} + \Omega] - \omega}{n\omega_d + n\Omega + [\alpha(m + nq) + l]\omega_b - i\nu_{eff} - \omega} \tag{10}$$

where ω_{*N}, ω_{*T} - diamagnetic frequencies associated with the equilibrium density and temperature gradients, respectively, ω_b - bounce frequency, ω_d - bounce averaged magnetic drift frequency, ν_{eff} - effective collision frequency, α =0 for trapped particles, and α =1 for passing particles. For passing particles, the bounce frequency ω_b becomes the transit frequency ω_t. The energy damping of the mode is associated with the singularity of the resonant operator, as the denominator vanishes. The finite mode growth (damping) rate and the collisionality term eliminate the singularity, and hence modifies the eventual damping energy. The collisionality effect on the RWM stability (via the collision frequency term $i\nu_{eff}$ of the resonant operator) is not considered in this

work, although the electron collision in RFP plasmas is probably high enough to have a large impact on the kinetic contribution from electrons.

Equations (1)-(9) form a MHD-kinetic hybrid system in a non-perturbative manner, where the eigenfunction (and the eigenvalue) is allowed to be self-consistently determined in the presence of kinetic effects.

The ion Landau damping of the parallel sound wave can be modeled by replacing the viscous stress tensor term from Eq. (2) by a parallel viscous force [26]

$$\nabla \cdot \Pi = \kappa |k_{\parallel} v_{thi}| \rho (\mathbf{v} \cdot \hat{\mathbf{b}} \hat{\mathbf{b}}) \tag{11}$$

where κ is a numerically tunable coefficient determining the damping strength. $k_{\parallel} = (n - m/q)/R$ is the parallel wave number. v_{thi} is the ion thermal velocity.

The system of the ideal single fluid equations can be recovered by dropping the parallel and the perpendicular kinetic pressure tensor terms, and adding the term $-5/3P\nabla \cdot \mathbf{v}$ to the right hand side of Eq. (4), to obtain the adiabatic equation of state.

The system of equations (1) - (9) is formulated as an eigenvalue problem, that can be written in a matrix form

$$-i\omega BX = A(\omega)X \tag{12}$$

where A, B represent the MHD operators, and X is the solution variables (the eigenvector). Note that the eigenvalue problem becomes nonlinear since the complex eigenfrequency ω enters into operator A via the resonant operator (10). This nonlinearity is resolved in the MARS-K code [36] by using an iterative algorithm with relaxation. At each iteration, an inverse iteration scheme is used to find the eigenvalue and eigenvector of Eq. (12).

The problem is solved in full toroidal geometry, in a flux coordinate system (s,χ,ϕ), where $s = \sqrt{\psi_p}$, with $\psi_p = |(\psi - \psi_0)|/|(\psi_a - \psi_0)|$ being the normalized poloidal flux (ψ_0 and ψ_a are the equilibrium poloidal flux on the magnetic axis and at the plasma boundary surface, respectively). χ is the generalized poloidal angle and ϕ is the geometrical toroidal angle. The equilibrium quantities are obtained by using the equilibrium solver CHEASE [37].

3. Equilibria specifications

We choose equilibria that closely model the typical RFX plasmas. We assume a circular plasma cross-section, with the major radius $R_0 = 2.0$ m and the inverse aspect ratio $\varepsilon = 0.23$. The global equilibrium parameters (for RFP) are $F \equiv B_\phi(a)/< B_\phi >$=-0.06, $\Theta \equiv B_\theta(a)/< B_\phi >$=1.41, where $B_\theta(a)$,$B_\phi(a)$ are the equilibrium poloidal and toroidal fields, respectively, at the plasma edge ($< \cdot >$ here denotes the average over the plasma column). The total plasma current is I_p=1.6 MA. The on-axis toroidal field is B_0=1.53 T. For comparative studies, we consider a set of equilibria, with a base case having the poloidal beta $\beta_p \equiv 8\pi < p > V_{tot}/I_p^2$=4%, corresponding to the on-axis electron and ion temperatures and densities T_{e0}=1 keV, T_{i0}=400 eV, $n_{e0} = n_{i0}$=2$\times$ 10^{19}

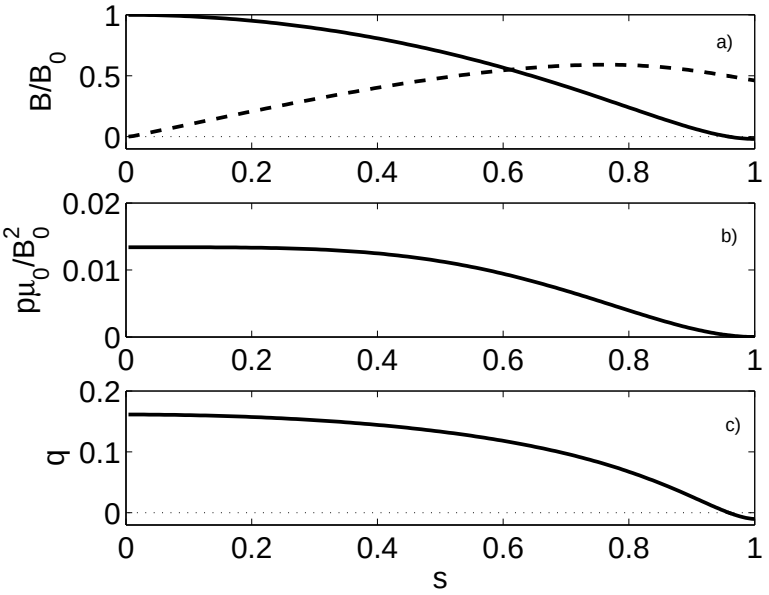

Figure 1. Equilibrium profiles along the minor radius $s \equiv \sqrt{\psi_p}$, with ψ_p being the normalized poloidal flux, for (a) the normalized equilibrium magnetic field components (solid -toroidal component, dashed - poloidal component), (b) the normalized plasma pressure, and (c) the safety factor q. B_0 is the toroidal field at the magnetic axis.

m^{-3}. Here $< p >$ is the plasma volume averaged equilibrium pressure. For the base case, the pressure profile $p(r) = n(r) * T(r)$ is given by specifying the density profile $n(r) = n_0(1 - (r/a)^6)$ and the temperature profile $T(r) = T_0(1 - (r/a)^3)$. The on-axis and edge values of the safety factor are q_0=0.161, q_a=-0.01 for the base case. Figure 1 shows the radial profiles of the poloidal and toroidal equilibrium fields, the pressure as well as the safety factor for the base case. Variations of the equilibrium parameters (mostly the pressure) will be introduced, when the stability results are reported in the next two Sections.

4. Stability following fluid models

The RWM spectrum in RFP is usually characterized by the presence of several unstable modes with different toroidal mode numbers n. The Fourier harmonics with different helicities (positive or negative toroidal mode numbers) are visible in the spectrum due to the edge reversal of the equilibrium toroidal field. Figure 2 shows the computed spectrum of unstable RWMs for the base case equilibrium described in Section 3, in the absence of both plasma rotation and kinetic effects. The mode with $n = -6$ is most unstable. In further discussions, the stability of the $n = -6$ mode will be considered if not otherwise stated.

The computed poloidal Fourier harmonics of the normal displacement ξ_n are shown in Fig. 3, for the $n = -6$ mode. The $m = 1$ poloidal harmonic is dominant. This points

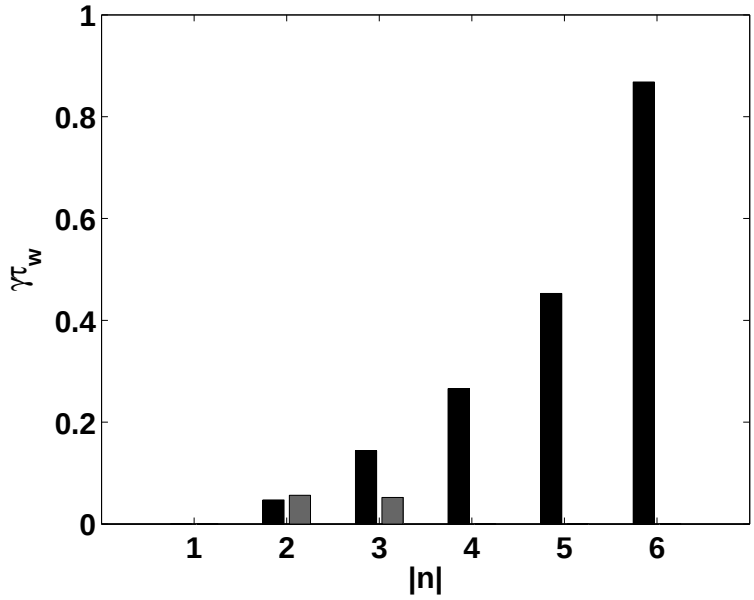

Figure 2. The MARS-F computed spectrum of the unstable RWMs for one of the RFX equilibria with $F = -0.06, \Theta = 1.41$ and $\Omega = 0$. The black color shows internal non-resonant modes with negative toroidal mode number $n < 0$. The grey color shows external non-resonant modes with $n > 0$. The poloidal harmonics are chosen as $m = 1, \cdots, 5$.

to a weak toroidicity induced coupling in RFP plasmas, even though the aspect ratio is just about 4.

Plasma rotation opens the possibility for the interaction of the otherwise static, non-resonant RWM with stable waves in the plasma. In ideal MHD, such interaction is due to the mode resonance with the continuum spectra. Two of them are known to be potentially in resonance with the RWM: the Alfvén continuum and the sound continuum. The condition for the resonance to occur can generally be written as $n\Omega+\omega_r = \omega_c$, where ω_c is either the Alfvén or the sound frequency. Note that both Ω and ω_c are generally functions of the plasma minor radius. For the static RWM ($\omega_r = 0$) the resonance condition becomes $n\Omega = \omega_c$. The mode resonance with the Alfvén continuum appears when the condition $|n\Omega| = |\omega_{ca}| \equiv |k_\parallel v_a|$ is satisfied. Here $v_a \equiv B/(\mu_0\rho)^{1/2}$ is the Alfvén velocity. Note that we neglected the $(1 + 2q^2)$ type of the Pfirsch-Schlueter inertia enhancement factor [27] in the above resonance condition. This factor is normally very close to unity for RFP plasmas. In order to demonstrate the effect of the pure Alfvén wave coupling, we consider a pressure-less equilibrium by setting $\beta_p = 0$ for the base case. Figure 4 shows the computed growth rate γ and frequency ω_r (both normalized by the wall time τ_w) of the fluid RWM, as we vary the plasma rotation frequency Ω. A uniform radial profile is assumed for the plasma rotation Ω.

Because of the absence of rational surfaces inside the plasma for the RWM in RFP, no resonance between the mode and the Alfvén waves is possible at vanishing

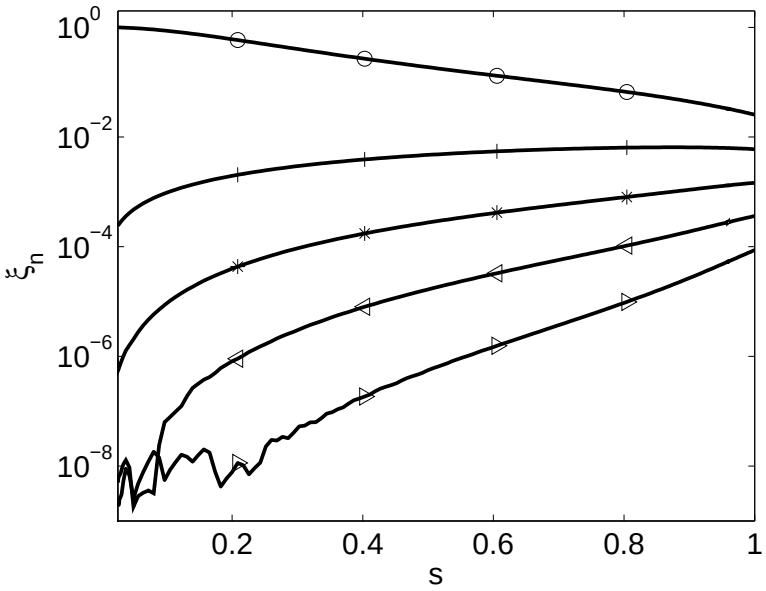

Figure 3. The radial profiles of the poloidal harmonics ($m = 1(o), m = 2(+), m = 3(*), m = 4(\triangleleft), m = 5(\triangleright)$) of the fluid RWM eigenfunction with $n = -6$. Plotted is the amplitude of the plasma normal displacement normalized by the maximum value in the straight field line coordinate system.

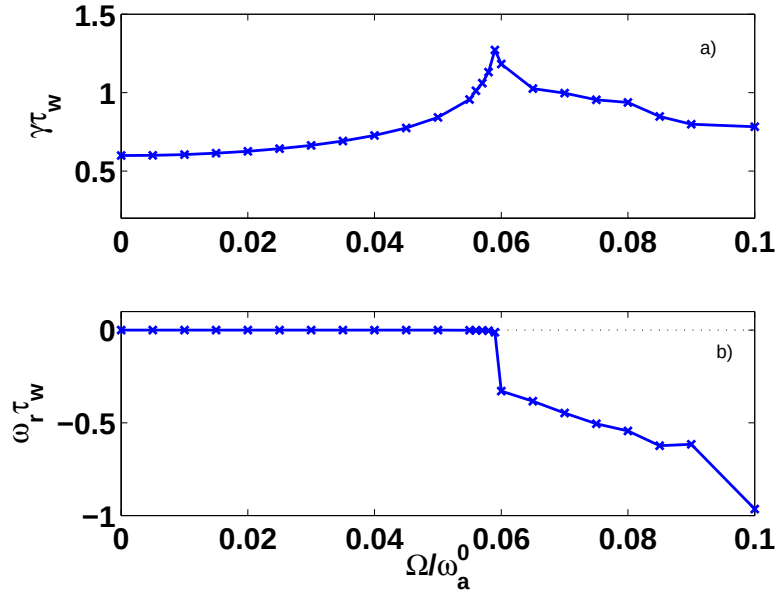

Figure 4. The computed (a) growth rate, and (b) frequency, of the fluid RWM in the presence of the Alfvén continuum resonance alone. The toroidal rotation frequency Ω, normalized by the Alfvén frequency ω_a^0 in the plasma center, is varied. The equilibrium is specified by $F = -0.06, \Theta = 1.41, \beta_p = 0$.

or sufficiently slow plasma rotation. The analytically predicted rotation frequency, at which the above described resonance condition starts to satisfy, is $\Omega = 0.06\omega_a^0$. Indeed, the numerical results start to show a resonant behavior at this rotation frequency. Specifically, the mode growth rate $\gamma\tau_w$ starts to decay for plasma rotation frequency $\Omega > 0.06\omega_a^0$, accompanied by the appearance of the finite mode frequency. This points to the damping effect from the mode-continuum resonance, though no compete RWM stabilization is achieved for the rotation range considered here. The critical rotation frequency, for the mode resonance to occur, is much less than that obtained in the previous study [34], due to the fact that we consider here the internal non-resonant RWM with $n = -6$. For this harmonic the resonant surface lies much closer to the plasma than that for the external non-resonant modes studied in [34]. At relatively slow rotation $\Omega > 0.06\omega_a^0$, the Alfvén resonance already starts to appear near the magnetic axis. It should be noted that the experimentally observed plasma rotation frequency in RFX ($\Omega \sim 10^{-3}\omega_a$ [38]) is much smaller than the value obtained here, for the mode resonance with the Alfvén continuum to occur.

The resonance of the RWM with parallel sound wave (more precisely the slow magneto-acoustic wave) appears when $n\Omega = \omega_{cs} \equiv k_\parallel v_s$ where $v_s = (\Gamma p/\rho)^{1/2}$ is the sound velocity ($\Gamma = 5/3$). In order to study this effect, we consider our base case with finite equilibrium pressure. The analytically predicted minimal rotation frequency, from which the above resonance condition starts to be satisfied, is $\Omega/\omega_a^0 = 0.005$. Figure 5 shows the computed fluid RWM eigenvalue versus rotation. The curves with "$\times$" shows the results without any other damping, such that the mode resonance with the parallel sound wave is the only possible damping term (in the range of rotation considered here). The change of the growth rate behavior occurs very close to the analytically predicted point $\Omega/\omega_a^0 = 0.005$. Also, the mode frequency becomes finite at this rotation frequency, indicating a damping term arising from the resonance. This study shows that the RFP equilibrium can provide a very "clean" understanding of the continuum damping physics for the RWM.

The initial destabilization phase of the RWM by rotation, shown by the curve with "$\times$" in Fig. 5, is due to an artifact of the ideal MHD model [25]. This is because the ideal MHD model (with adiabatic equation of state) cannot describe adequately the particle motion along the magnetic field lines, causing unphysical destabilization effect of the mode by the subsonic flow. A rigorous treatment should invoke kinetic description for the parallel motion of particles. However, a reasonable fluid-like damping term, Eq. (11), first introduced in Ref. [26], helps to remove this unphysical destabilization behavior, by damping the parallel sound wave in the ideal MHD model.

By tuning the numerical coefficient κ in Eq. (11), we can vary the damping strength for the parallel sound wave, and hence the RWM stability. The numerical results are shown in Fig. 5 by choosing various values of κ. At sufficiently large κ, the destabilization effect by plasma rotation disappears. Further increase of κ leads to more suppression of the mode by the plasma rotation.

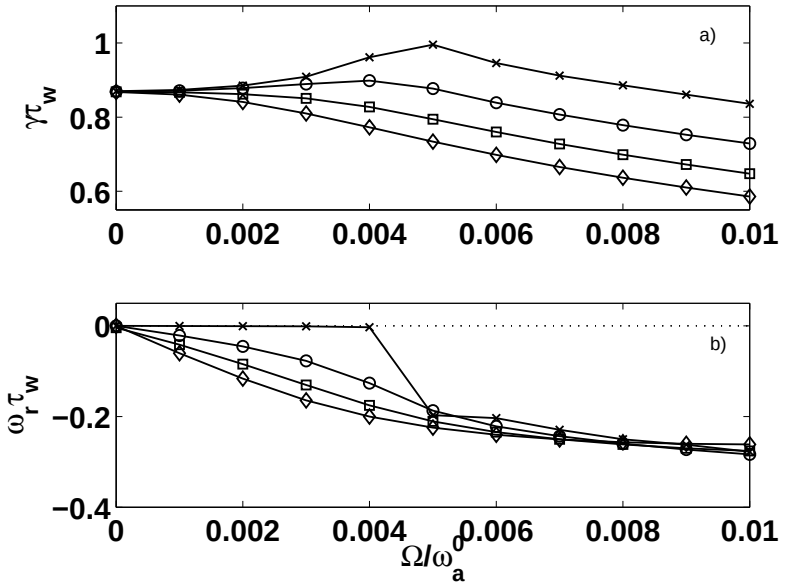

Figure 5. The computed (a) growth rate, and (b) frequency, of the fluid RWM in the presence of the sound wave continuum resonance. The toroidal rotation frequency Ω, normalized by the Alfvén frequency ω_a^0 in the plasma center, is varied. The equilibrium is specified by $F = -0.06, \Theta = 1.41, \beta_p = 4\%$. The strength of the parallel sound wave damping is varied by choosing κ=0.0 ('×'), κ=0.5 ('o'), κ = 1.0 ('□'), and κ = 1.5 ('◇').

5. Stability following kinetic models

5.1. Effects of various kinetic resonances

Whilst the stability of an ideal kink mode, growing at the Alfvén time scale, is normally well described by ideal MHD theory, the stability of the RWM, that often grows at the drift wave time scale, is better described by kinetic theory, due to the (possibly strong) mode resonance with drift motions of bulk plasma particle species. In MARS-K, these resonant effects are introduced into MHD through the pressure tensors (6) with the resonant operator (10).

Equations (7)-(10) show that the resonance can occur with different types of particle drifts, depending on the plasma rotation frequency. In this work, we consider the mode resonance with both precessional drifts and bounce motions of thermal particles. We also consider contributions from different plasma species (electrons and ions). Generally the local value of the particle drift frequencies (even after the bounce average) can have complicated dependence on the particle pitch angle Λ and the particle kinetic energy ϵ_k, at each flux surface. The total effect of the mode-particle resonances is obtained by computing the above mentioned local frequencies. On the other hand, some qualitative understanding can be reached by comparing the particle distribution averaged bounce and precession frequencies, which are shown in Fig. 6 for thermal ions, for the base case

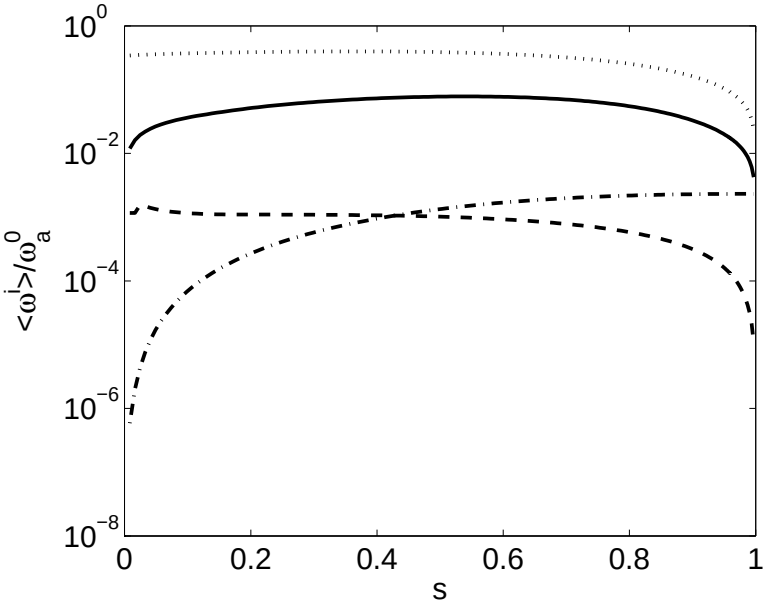

Figure 6. The radial profiles of drift frequencies for thermal ions, averaged over the particle equilibrium distribution function. Compared are the normalized (to the central Alfvén frequency ω_a^0) frequencies among the bounce frequency ω_b of trapped ions (solid), the transit frequency ω_t of passing ions (dotted), the magnetic precession frequency ω_d of trapped ions (dashed), and the thermal ion diamagnetic frequency ω_* (dash-dotted). The RFX equilibrium is chosen with $F = -0.06, \Theta = 1.41, \beta_p = 4\%$.

equilibrium.

Figure 6 compares the averaged transit frequency ω_t for passing ions, the bounce frequency ω_b for trapped ions, the magnetic precession frequency ω_d for trapped ions, as well as the ion diamagnetic frequency ω_*, defined here as the sum of the contributions from both density and temperature gradients. The experimental plasma rotation frequency $\Omega_{\rm exp}$, not shown in the figure, is calculated as in the order of 0.1% of the Alfvén frequency in RFX [38], and hence being comparable to the thermal particle magnetic precession frequency $\Omega_{\rm exp} \sim \omega_d$. The following ordering of frequencies is valid for the studied case here

$$\omega_r \ll \Omega_{\rm exp} \sim \omega_d \sim \omega_* \ll \omega_b \sim \omega_s^{i0} < \omega_{ca} < \omega_t < \omega_a^0 \tag{13}$$

where $\omega_s^{i0} \simeq 0.1\omega_a^0$ is the central ion sound frequency.

In this work we assume subsonic rotation $\Omega \lesssim \omega_s^{i0}$. In particular, we consider two sub-regions in view of the above ordering, namely $\Omega \sim \omega_d$ and $\omega \sim \omega_b$. In each of these sub-regions, we expect certain kinetic effects on the RWM stability, due to the mode-particle resonances.

Before showing numerical results, it is useful to make a qualitative estimate of the kinetic contribution from different sorts of particles (trapped/passing, ions/electrons) in different rotation regimes, based on the resonant operator (10). We shall neglect the mode frequency ω and the collisionality term $\nu_{\rm eff}$ for this analysis. We carry out the

analysis for the $n = -6$ mode.

In the sub-region $\Omega \sim \omega_d$, for trapped particles ($\alpha = 0$), we have $\lambda \sim (\omega_* + \Omega)/(\omega_d + \Omega + (l/n)\omega_b)$. At $l = 0$, the mode resonance with magnetic precession drift motion of trapped ions and electrons becomes dominant. At $l \neq 0$, the resonance condition requires that $\omega_d \sim (l/n)\omega_b$, which cannot be satisfied in most of plasma regions, since $\omega_d/\omega_b \approx 0.02$ for ions, following Fig. 6. However, this resonance can be satisfied locally in the plasma core and edge regions, where $\omega_d \sim \omega_b$. The resonance with the electron bounce motion should be even smaller due to much larger bounce frequency for electrons.

For passing ions ($\alpha = 1$) in the sub-region $\Omega \sim \omega_d$, the resonance can occur only if $(m + nq + l)/n \sim \omega_d/\omega_t$. Since $|\omega_d/\omega_t| < 10^{-2}$ for the case studied here, the resonant contribution from passing particles can only be expected locally near the reversal radius of the safety factor $|q| \ll 1$ and when $m + l = 0$.

Therefore, in the low rotation frequency sub-region, we expect that the major effect on the RWM stability comes from the mode resonance with the magnetic precession drift of trapped ions and electrons. The contributions from bounce or transit motion of thermal ions are always localized along the minor radius and hence being small.

In the sonic rotation sub-region $\Omega \sim \omega_b$, the particle magnetic precession does not play a significant role, since $\omega_d \ll \omega_b$. For trapped particles (ions), $\lambda \sim (\omega_* + \Omega)/((l/n)\omega_b + \Omega)$, the resonance condition is satisfied when $(l/n)\omega_b \simeq -\Omega$, for $l \neq 0$. For the $n = -6$ mode, the bounce harmonic with $l = 6$ should give the dominant contribution. The lower l harmonics can also play a larger role with decreasing Ω.

The resonance condition is more intriguing for passing ions in the sonic rotation regime, in which $\lambda \sim (\omega_* + \Omega)/[\omega_t(m + nq + l)/n + \Omega]$. The resonance occurs when $(m + nq + l)/n \sim \omega_b/\omega_t$. Since $|\omega_b/\omega_t| \sim 0.1$ for our plasma, the contribution of passing particles can be expected for a larger region near the field reversal surface, i.e. $|q| \lesssim 0.1$ and $m + l = 0$. [Note that the present equilibrium has $|q| < 0.16$ in the whole plasma region.]

We conclude that both trapped and passing ions can contribute to the kinetic resonances, for the plasma rotation frequency in the order of the ion sound frequency. The trapped particle contribution comes from the bounce motion with specific bounce harmonics. The passing particle contribution can come from a broad region near the field reversal surface. The latter is different from the case of the slow rotation regime $\Omega \sim \omega_d$.

Now we turn to numerical results. Figure 7 reports the computed eigenvalue of the kinetic RWM versus rotation, using the full kinetic model (i.e. including resonance with all particles). For comparison, we also plot the fluid result with the parallel sound wave damping model (with the damping coefficient $\kappa = 1$). The kinetic model gives slightly lower growth rate at low rotation frequency ($\Omega \lesssim \omega_d$), whilst a stronger suppression is obtained, at $\Omega \sim \omega_b$, by using the viscous damping model. Further increase of the plasma rotation ($\Omega > 0.05\omega_a^0$) leads to a slight destabilization of the mode with both damping models. For the kinetic model, this is due to the loss of resonances. For the

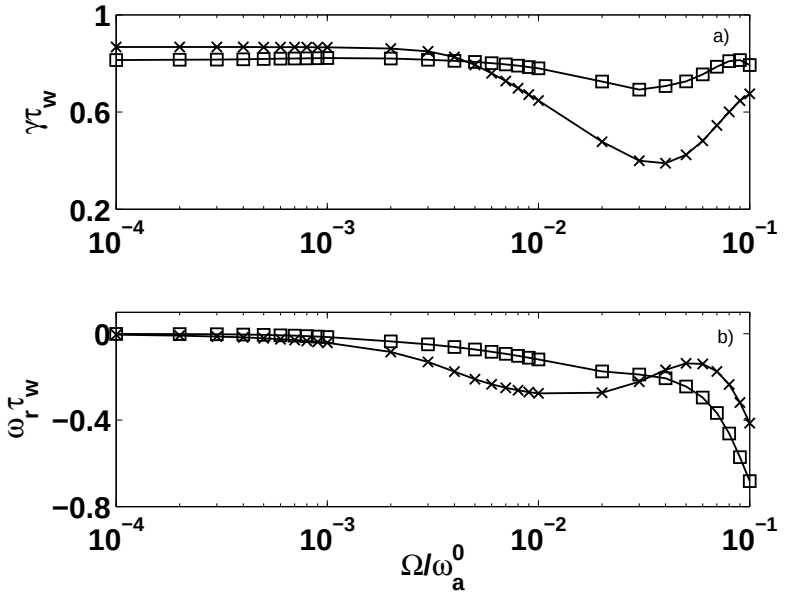

Figure 7. Compare (a) the growth rate, and (b) the frequency, of the RWM between the parallel sound wave damping model with $\kappa = 1.0$ ('×'), and the full kinetic damping ('□'). The toroidal rotation frequency Ω, normalized by the Alfvén frequency ω_a^0 in the plasma center, is varied. The equilibrium is specified by $F = -0.06, \Theta = 1.41, \beta_p = 4\%$.

viscous damping model, this is probably due to the imperfection of the model. Over the whole rotation regime considered here, the kinetic model generally does not predict a significant stabilization of the RWM for the RFX plasma. In fact, in the (slow) rotation regime relevant to the RFX plasma, the relative change of the mode growth rate, introduced by the bulk particle kinetic effects, is less than 5% in our case.

We point out that our kinetic formulation effectively replaces the adiabatic equation of state, in the ideal MHD model, by the kinetic pressure closure. By doing so, we eliminate the unphysical coupling of the mode to the parallel sound wave, and hence remove the destabilization effect by the sound wave at subsonic rotation, as observed in Fig. 5.

Further numerical results compare kinetic contributions from different kinetic resonances and particle fractions, by artificially switching off terms from the resonance operator (10). Figure 8 compare the computed mode eigenvalues by retaining all terms (the full model), the bounce resonance terms only, and the precession resonance terms only. Both trapped and passing particles are included. From the qualitative discussions performed above, we understand that when the precessional resonance alone is included, the passing particle contribution does not have much physical effect. We nevertheless consider this as a "numerical" option.

Two plasma rotation regimes can again be distinguished, separated by the value of $\Omega/\omega_a^0 \approx 10^{-2}$. In the region of $\Omega/\omega_a^0 < 10^{-2}$, the computed eigenvalues using the full model closely follow that assuming the precessional drift resonance alone. The mode

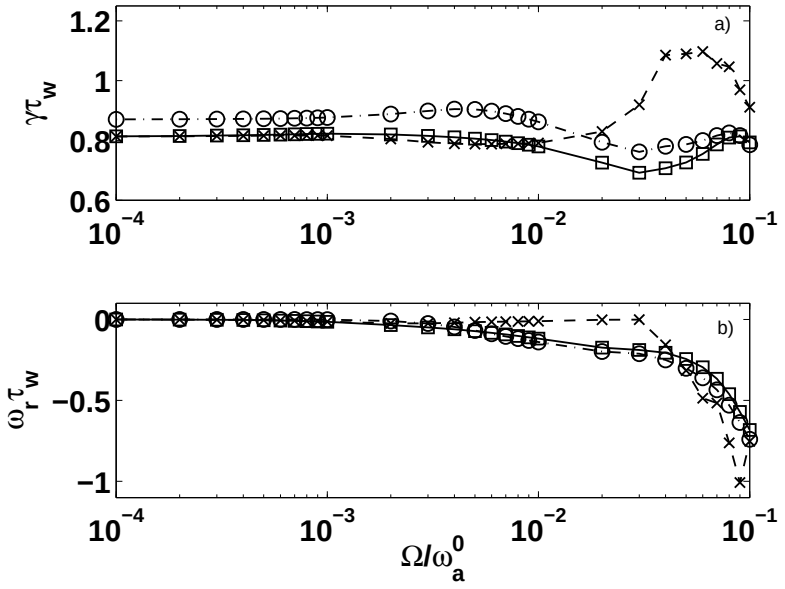

Figure 8. The computed (a) growth rate, and (b) frequency, of the kinetic RWM, including the mode resonance with the particle precession frequency alone ('×'), with the particle bounce-transit frequency alone ('o'), and with both frequencies ('□'). Both trapped and passing particles are included. The toroidal rotation frequency Ω, normalized by the Alfvén frequency ω_a^0 in the plasma center, is varied. The equilibrium is specified by $F = -0.06, \Theta = 1.41, \beta_p = 4\%$.

growth rate for these two cases is slightly less than that with the bounce resonance alone, indicating a small but finite damping effect from the precessional resonance. In the region of $\Omega/\omega_a^0 > 10^{-2}$, the situation becomes opposite: the eigenvalues from the full model follow well that with the bounce resonance alone, indicating that the major kinetic effects come from the mode resonance with particle transit and/or bounce motions. The growth rate peaking near $\Omega/\omega_a^0 \simeq 5\times10^{-2}$, with the precessional resonance alone, can be attributed partially to the loss of the resonance condition, and partially to the behavior associated with the Alfvén continuum resonance, as observed in Fig. 4.

Figure 9 compares the kinetic results for trapped particles only. The computed mode growth rate, with the precessional resonance alone, follows well the "full" model (i.e. with both precession and bounce resonances for trapped particles in this case), for the plasma rotation frequency Ω up to about $5 \times 10^{-2}\omega_a^0$. In the region between $1-5\times10^{-2}\omega_a^0$, we do not expect much resonance damping due to the particle precession. Most likely, the stabilizing effect from the particle precession, as shown in the figure, comes from the real part of the kinetic energy in this frequency range, i.e. from the inertial effect. It is also clear from Fig. 6, that the inertial effect comes primarily from the particle precession, rather than from the bounce/transit motions, due to the fact that the diamagnetic flow is comparable to the precession frequency, but much smaller than the bounce/transit frequencies.

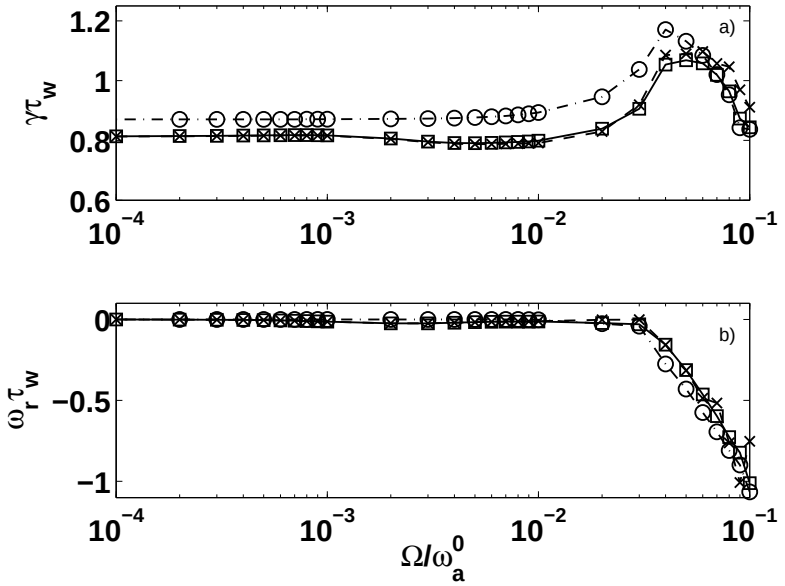

Figure 9. The computed (a) growth rate, and (b) frequency, of the kinetic RWM, including the mode resonance with the particle precession frequency alone ('×'), with the particle bounce-transit frequency alone ('o'), and with both frequencies ('□'). Only trapped particle contribution is included. The toroidal rotation frequency Ω, normalized by the Alfvén frequency ω_a^0 in the plasma center, is varied. The equilibrium is specified by $F = -0.06, \Theta = 1.41, \beta_p = 4\%$.

When the plasma rotation frequency starts to match or exceed the trapped particle bounce frequency, $\Omega \gtrsim 5 \times 10^{-2}\omega_a^0$, figure 9 shows that the computed growth rate, with the bounce resonance alone, starts to follow the "full" model, indicating that the bounce resonance damping of trapped particles starts to play a dominant role. We mention that the mode resonance with the Alfvén continuum also starts to play a role in this rotation regime.

Summarizing Figs. 8 and 9, we find that, in the slow rotation regime $\Omega < 10^{-2}\omega_a^0$, most of the kinetic effect comes from the mode resonance with particle precession. In the fast rotation regime $\Omega > 5 \times 10^{-2}\omega_a^0$, the kinetic effect from trapped particle bounce motions prevails. In the regime between $10^{-2}\omega_a^0 < \Omega < 5 \times 10^{-2}\omega_a^0$, both precessional drift of trapped particles (inertial effect), and the transit motion of passing particles (resonant damping effect) can contribute. But not much damping effect is observed from the bounce motion of trapped particles. In this intermediate rotation regime, the dominant resonant contribution from passing particles' transit motion agrees with the qualitative analysis (the effect of large radial resonance region with $|q| < 0.1$) made earlier in this Section. We point out that this passing particle resonance effect is rather specific to the RFP plasmas, and not to be expected in tokamak plasmas.

5.2. Effects of equilibrium pressure on kinetic results

Since the drift kinetic energy depends on both the equilibrium pressure amplitude and profile, we consider here how the pressure variation affects the growth rate of the kinetic RWM, following a similar study pursued for the tokamak plasma [39].

The shape of the pressure profile mostly affects the diamagnetic terms in the mode-particle resonance operator (10). We consider here two pressure profiles: one is specified in the base case equilibrium in Section 3, and used in the numerical computations described so far; the other is specified by the following density and temperature profiles, producing a more flat pressure profile: $n^{i,e}(r/a) = n_0^{i,e}(1-(r/a)^{12})$, $T^{i,e}(r/a) = T_0^{i,e}(1-(r/a)^6)$.

Figure 10 compares the results. The major change, in terms of the fluid and drift frequencies, is naturally the diamagnetic frequency ω_*, as shown in Fig. 10(b). Note also slight changes of the averaged magnetic precession frequency ω_d and the transit frequency ω_t of passing particles (ω_t is normalized by the factor 0.01). The bounce frequencies of trapped particles are not compared here, since the bounce resonance does not seem to make a significant contribution to the mode stability (see Figs. 8 and 9).

In terms of the mode stability, the flat pressure profile in the core is slightly less stabilizing than the more peaked profile, in the slow rotation regime $\Omega \sim \omega_d \sim 10^{-3}\omega_a^0$, as shown in Fig. 10(c). [Note that, since the change of equilibrium pressure also results in a slight change of the fluid growth rate for the RWM, we compare here the kinetic growth rates, both normalized to unity at vanishing rotation.] This should be due to a smaller ω_* value with the flat profile in the core. Similar effect is observed at the high rotation end $\Omega \gtrsim 2\times 10^{-2}\omega_a^0$. The flat profile, however, is slightly more stabilizing for the intermediate rotation. Probably due to a combined effect caused by the trapped particle precession and passing particle transit motion. We emphasize that these explanations here are rather qualitative. The eventual comparison, as shown in Fig. 10(c-d), is the integrated effect of all inertial and resonant effects, with both passing and trapping particles.

The amplitude of the plasma pressure, β_p, acts as a linear scaling factor to both the diamagnetic and precessional drift frequencies. The particle bounce frequency scales as the square root of β_p. We shall perform a broad scan of the plasma pressure amplitude, with β_p =5%, 15% and 25%. In order to separate the kinetic bounce resonance effect from the Alfvén continuum resonance, both occurring at $\Omega \simeq 6 \times 10^{-2}\omega_a^0$ for the base case studied before for the $n = -6$ mode, we shall now consider the $n = -5$ mode, for which the Alfvén resonance occurs at much larger rotation frequency $\Omega \simeq 0.2\omega_a^0$. We thus can neglect the Alfvén resonance effect for the rotation frequency range of $\Omega = 0 - 0.1\omega_a^0$, that we choose to study the kinetic effects.

Figure 11 summarizes the results. To compare the relative effect of the kinetic (de-)stabilization (and to remove the fluid effect of the pressure amplitude), we again normalize the growth rate to unity at vanishing rotation, as shown in Fig. 11(c). With this normalization, the essential effect of increasing the equilibrium pressure is to shift

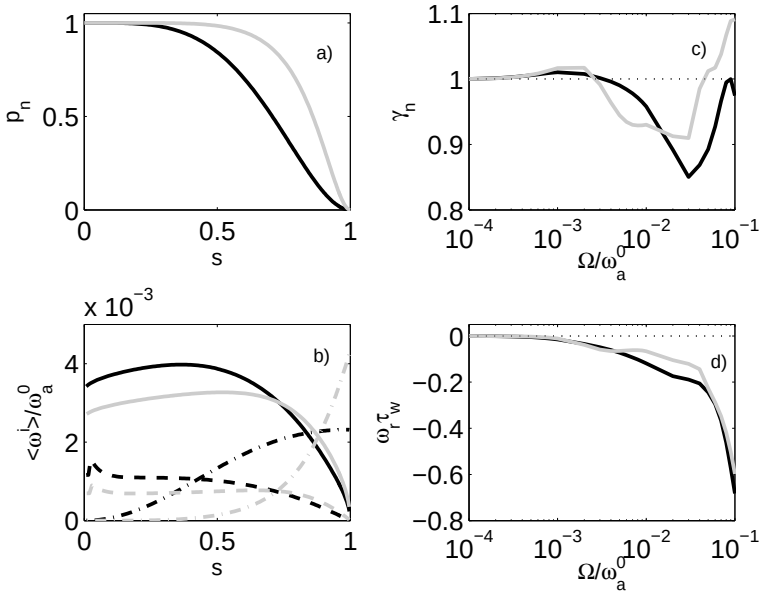

Figure 10. Effects of equilibrium pressure profiles on the stability of the kinetic RWM. Plotted are (a) the normalized radial profiles of pressure; (b) the distribution function averaged drift frequencies (solid - $\omega_t * 0.01$, dashed - ω_d, dashed-dotted - ω_*); (c) the mode growth rate (normalized to unity at vanishing rotation) and (d) the mode frequency versus the normalized plasma rotation frequency. The black curves correspond to the case with $n(r) = n_0(1-(r/a)^6), T(r) = T_0(1-(r/a)^3)$. The grey curves correspond to the case with $n(r) = n_0(1-(r/a)^{12}), T(r) = T_0(1-(r/a)^6)$.

both the precessional and bounce resonances to larger rotation frequency, as evident from the resonance operator (10). This is also confirmed by the numerical results shown in 11(c). The effect is more prominent for the particle bounce resonance. We mention that such a large shift of resonance condition normally does not occur for tokamak plasmas, since the range of variation of the equilibrium thermal pressure is normally much smaller, between the no-wall and the ideal-wall beta limits (much smaller than the factor of 5 as we assumed in this study).

5.3. Ion versus electron contributions

The total thermal pressure consists of the ion and electron contributions. With the same equilibrium pressure, the drift kinetic energy depends on the ion-electron temperature ratio. Following a similar study for tokamaks [36], we consider here the role of relative contribution from ions and electrons, on the RWM stability in RFP plasmas.

We consider the precessional drift resonance alone, since only this type of resonance gives comparable contributions from thermal ions and electrons. The kinetic contribution from bounce resonance of electrons is much smaller that of the ion contribution, and hence is normally neglected in the kinetic study. We define a figure of

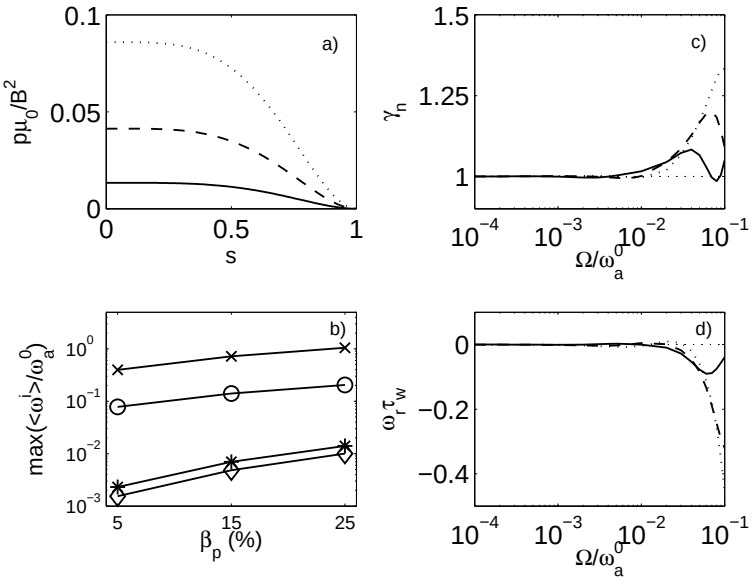

Figure 11. Effects of equilibrium pressure amplitude on the stability of the kinetic RWM. Plotted are (a) the radial pressure profiles; (b) the maximum of the averaged drift frequencies as a function of poloidal beta ($\omega_t(\times)$, ω_b(o), $\omega_*(*)$ $\omega_d(\diamondsuit)$); (c) the mode growth rate (normalized to unity at vanishing rotation) and (d) the mode frequency versus the normalized plasma rotation frequency. Compared are three cases with β_p=5% (solid), β_p=15% (dashed), and β_p=25% (dotted).

merit $C_p \equiv T_{i0}/(T_{i0}+T_{e0})$. If we further assume that the bulk ions and electrons have the same density, and the same temperature profile, it can be easily worked out, based on the resonance operator (10), that the total kinetic contribution, from both ions and electrons, does not depend on the direction of the plasma rotation if $C_p = 0.5$. This is confirmed by the numerical results shown in Fig. 12, where the eigenvalues of the $n = -6$ kinetic RWM are compared using the base case equilibrium. However, when $C_p \neq 0.5$, this symmetry (with respect to the sign of Ω) is broken. Indeed, assuming $C_p = 0.33$, corresponding to T_{e0}=1keV and T_{i0}=0.5 keV in the present study, the mode growth rate behaves differently with positive and negative rotation directions. With negative Ω, the mode stabilization effect is observed at lower rotation speed, than that with positive Ω. This is qualitatively understandable. Since $|\omega_d| \propto T$, $|\omega_d^i| < |\omega_d^e|$. On the other hand, the negative rotation leads to a predominant resonance damping with trapped ions (not electrons), according to Eq. (10) and Fig. 6. Therefore, with increasing $|\Omega|$, the mode resonance first occurs with trapped ions, which has smaller precession frequency. We notice that, whilst this qualitative analysis explains well the numerical results here for the RFP plasmas, it may not always work for tokamak plasmas, due to the precession reversal effect occurring for both ions and electrons. This precession reversal is often substantially enhanced by the finite pressure effect in the tokamak field geometry.

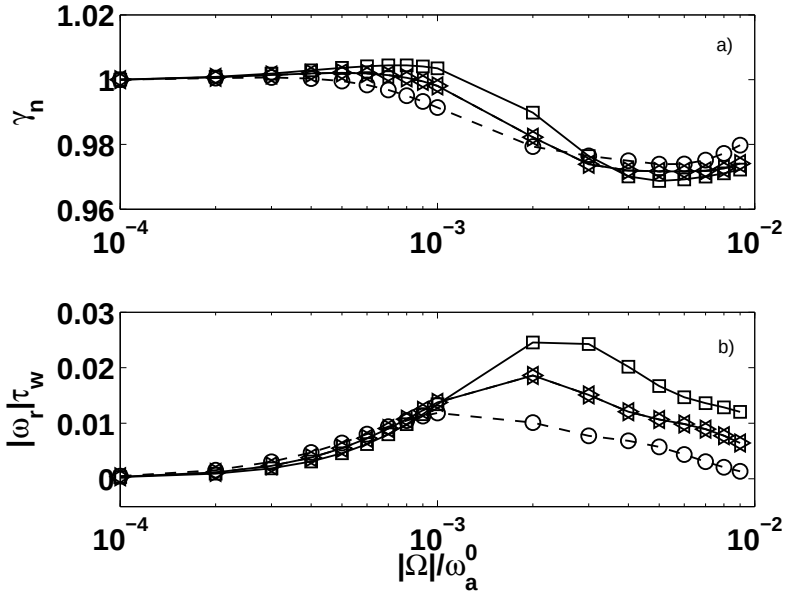

Figure 12. Relative contributions of thermal ions/electrons, as well as the effect of the rotation direction, on the RWM stability. Plotted are (a) the mode growth rate, and (b) the mode frequency, for various cases: $\Omega > 0, C_p = 0.33$ (solid line with "□"), $\Omega > 0, C_p = 0.5$ (solid line with "◁"), $\Omega < 0, C_p = 0.33$ (dashed line with "o"), $\Omega < 0, C_p = 0.5$ (dashed line with "▷"). The mode growth rate is normalized to unity at $\Omega = 10^{-4}\omega_a^0$, for all cases. Absolute value of the mode frequency is plotted.

6. Conclusion and discussion

We have carried out systematic study of the drift kinetic effects on the RWM stability in RFP plasmas, using the MARS-K code with a non-perturbative MHD-kinetic hybrid formulation. Both magnetic precession and transit-bounce motions of thermal ions and electrons are considered. A wide range of the plasma rotation and pressure scans has been performed. The kinetic results are compared with the fluid results.

One of the main results of the present numerical investigation, is that the drift kinetic effects do not substantially modify the RWM growth rate for RFP plasmas, within the plasma rotation regime (generally subsonic) considered in this study. In fact the change of the mode growth rate, due to kinetic effects, is generally less than 5% compared to the fluid theory prediction, for the typical RFX plasma in the range of the experimental plasma rotation. This partially explains why the previous fluid computations [41] seem to match well the experimentally measured mode growth rates in RFX.

This numerical result can be qualitatively understood by comparing the perturbed drift kinetic energy with the perturbed fluid potential energy. For a current driven RWM, such as that in RFP plasmas, the drift kinetic energy is normally small compared to the fluid energy, and hence offering minor modification to the mode growth rate. For

pressure driven RWMs, especially those from the tokamak experiments, the drift kinetic energy can be comparable to the fluid energy, thus often resulting in a substantial modification of the mode stability, compared to the fluid prediction [40].

Another interesting result from the present study, is the observation that, at the plasma rotation of the order of the sound speed, the kinetic effect on the RWM mainly comes from the transit resonance of *passing particles*. Not much kinetic effect is observed from the bounce motion of trapped particles, unless the plasma flow speed starts to exceed the sound speed. The transit resonance with passing particles occurs in a broad range of minor radius, where $|q| \lesssim 0.1$. This is a specific feature of RFP equilibria.

Both the computed kinetic and fluid mode growth rates can be relatively easily explained by analytic considerations. The former agrees well with the estimate from the kinetic resonance operator. The latter agrees with the continuum wave damping theory. Compared to the (sometimes complicated) kinetic effects in tokamak plasmas, the RFP magnetic configuration seems to give more transparent understanding of the RWM physics in many aspects, as also evident from the present numerical investigation.

We did not consider the kinetic effects from energetic particles for these RFP plasmas. In RFX experiments, some fraction of energetic particles can be induced by the neutral beam heating. We also neglected the effect of the plasma collisionality in this study. For RFX plasmas, the plasma collisionality, especially for electrons, is probably un-negligible, and need to be taken into account in the future study. As a final remark, we point out that our drift kinetic formalism is valid only for subsonic flow. Therefore, those kinetic results, where the plasma flow speed approaches the sound speed, should be treated with caution.

References

[1] Garofalo A M *et al* 1999 *Phys. Rev. Lett* **82** 3811
[2] Gryaznevich M *et al* 2003 *Bull. Am. Phys. Soc.* **48** 307
[3] Shilov M *et al* 2004 *Phys. Plasmas*, **11** 2573
[4] B Alper B *et al* 1989 *Plasma Phys. Controlled Fusion* **31** 205
[5] Brunsell P R *et al* 2003 *Phys. Plasmas* **10** 3823
[6] Bolzonella T *et al* 2005 Proceedings of the 32nd EPS Plasma Physics Conference (Tarragona) ECA (European Physical Society, Mulhouse Cedex, France, 2005) **29C** 1.107
[7] Bishop C M 1989 *Plasma Phys. Controlled Fusion* **31** 1179
[8] Fitzpatrick R and Jensen T H 1996 *Phys. Plasmas* **3** 2641
[9] Okabayashi M *et al* 1998 *Nucl. Fusion* **38** 1607
[10] Fitzpatrick R and Yu E P 1999 *Phys. Plasmas* **6** 3536
[11] Liu Y Q *et al* 2000 *Phys. Plasmas* **7** 3681
[12] Fransson M *et al* 2000 *Phys. Plasmas* **7** 4143
[13] Pustovitov V D *et al* 2001 *Plasma Phys. Rep.* **27** 195
[14] Liu Y Q *et al* 2006 *Phys. Plasmas* **13** 056120
[15] Okabayashi M *et al* 2001 *Phys. Plasmas* **8** 2071
[16] Strait E J *et al* 2004 *Phys. Plasmas* **11** 2505
[17] Sabbagh S A *et al* 2006 *Phys. Rev. Lett.* **97** 045004
[18] Brunsell P R *et al* 2004 *Phys. Rev. Lett.* **93** 225001
[19] Paccagnella R *et al* 2006 *Phys. Rev. Lett.* **97** 075001

[20] Reimerdes H *et al* 2006 *Phys. Plasmas* **13** 056107
[21] Gregoratto D *et al* 2001 *Plasma Phys. Controlled Fusion* **43** 1425
[22] Zheng L J *et al* 2005 *Phys. Rev. Lett.* **95** 255003
[23] Bondeson A and Ward D J 1994 *Phys. Rev. Lett.* **72** 2709
[24] Betti R and Freidberg J P 1995 *Phys. Rev. Lett* **74** 2949
[25] Bondeson A and Iacono R 1989 *Phys. Fluids B* **1** 1431
[26] Chu M S *et al* 1995 *Phys. Plasmas* **2** 2236
[27] Bondeson A and Chu M S 1996 *Phys. Plasmas* **3** 3013
[28] Liu Y Q *et al* 2005 *Nucl. Fusion* **45** 1131
[29] Menard J E *et al* 2010 *Nucl. Fusion* **50** 045008
[30] Bo Hu and Betti R 2004 *Phys. Rev. Lett.* **93** 105002
[31] Reimerdes H *et al* 2007 *Phys. Rev. Lett.* **98** 055001
[32] Berkery J W *et al* 2010 *Phys. Plasmas* **17** 082504
[33] Jiang Z X *et al* 1995 *Phys. Plasmas* **2** 442
[34] Guo S C *et al* 1999 *Phys. Plasmas* **6** 3868
[35] Sonato P *et al* 2003 *Fusion Eng. Des.* **66** 161
[36] Liu Y Q *et al* 2008 *Phys. Plasmas* **15**, 112503
[37] Lütjens H *et al* 1996 *Comp. Phys. Commun.* **97** 219
[38] Guazzotto L and Paccagnella R 2009 *Plasma Phys. Controlled Fusion* **51** 065013
[39] Liu Y Q *et al* 2008 *Phys. Plasmas* **15** 092505
[40] Liu Y Q *et al* 2009 *Phys. Plasmas* **16** 056113
[41] Villone F *et al* 2008 *Phys. Rev. Lett.* **100** 255005